





**BRIEF DEFINITIVE REPORT**

# Gene therapy targeting SARM1 blocks pathological axon degeneration in mice

Stefanie Geisler<sup>1,4</sup> , Shay X. Huang<sup>1</sup>, Amy Strickland<sup>2</sup>, Ryan A. Doan<sup>1</sup> , Daniel W. Summers<sup>2</sup>, Xianrong Mao<sup>2</sup>, Jiwoong Park<sup>2</sup>, Aaron DiAntonio<sup>3,4</sup> , and Jeffrey Milbrandt<sup>2,4</sup> 

**Axonal degeneration (AxD) following nerve injury, chemotherapy, and in several neurological disorders is an active process driven by SARM1, an injury-activated NADase. Axons of SARM1-null mice exhibit greatly delayed AxD after transection and in models of neurological disease, suggesting that inhibiting SARM1 is a promising strategy to reduce pathological AxD. Unfortunately, no drugs exist to target SARM1. We, therefore, developed SARM1 dominant-negatives that potently block AxD in cellular models of axotomy and neuropathy. To assess efficacy in vivo, we used adeno-associated virus-mediated expression of the most potent SARM1 dominant-negative and nerve transection as a model of severe AxD. While axons of vehicle-treated mice degenerate rapidly, axons of mice expressing SARM1 dominant-negative can remain intact for >10 d after transection, similar to the protection observed in SARM1-null mice. We thus developed a novel in vivo gene therapeutic to block pathological axon degeneration by inhibiting SARM1, an approach that may be applied clinically to treat manifold neurodegenerative diseases characterized by axon loss.**

## Introduction

Axonal degeneration (AxD) is an early, potentially initiating event in prevalent neurological diseases including peripheral neuropathies, traumatic brain injury, Parkinson's disease, and glaucoma (Howell et al., 2013; Johnson et al., 2013; Cashman and Höke, 2015; Tagliaferro and Burke, 2016). Although AxD is central to many neurological disorders, no treatments currently exist that effectively target axon breakdown.

Axon degeneration is a genetically encoded program of subcellular self-destruction. Two large-scale forward genetic screens, one in invertebrates and one in mammals, independently identified a crucial role for sterile  $\alpha$  and TIR (Toll-like interleukin 1 receptor) motif-containing protein 1 (SARM1) in this endogenous AxD program (Osterloh et al., 2012; Gerdts et al., 2013). Genetic deletion of SARM1 preserves *Drosophila* olfactory bulb distal axons for >50 d after a cut and mouse sciatic distal segments for >2 wk after transection. SARM1 is not only necessary for AxD but is also sufficient (Gerdts et al., 2015). Activation of SARM1 in healthy axons results in AxD, even in the absence of injury, thus indicating a fundamental role for SARM1 in the AxD program (Gerdts et al., 2016).

Genetic deletion of SARM1 protects axons from degeneration not only after a cut but also in models of several neurological diseases, including peripheral neuropathies (Geisler et al., 2016;

Turkiew et al., 2017) and traumatic brain injury (Henninger et al., 2016; Ziogas and Koliatsos, 2018). This axon protection is associated with greatly improved functional outcomes, suggesting that targeting SARM1 is a viable strategy to treat neurological diseases characterized by early AxD. Importantly, SARM1 is expressed mainly in neurons, and SARM1 KO mice have a normal lifespan and no overt behavioral abnormalities, suggesting that targeting SARM1 may be well tolerated. Unfortunately, there are currently no known drugs that inhibit SARM1 activity.

SARM1 is a multidomain protein that consists of an autoinhibitory N terminus, tandem SAM domains that mediate constitutive homomultimerization, and an executioner TIR NADase domain (Gerdts et al., 2013, 2016; Essuman et al., 2017). Upon injury, N-terminal inhibition is relieved, allowing for TIR-TIR interactions that activate the intrinsic NADase enzyme, thereby cleaving the essential metabolic cofactor NAD<sup>+</sup> and driving AxD (Gerdts et al., 2016; Essuman et al., 2017). Because SARM1 exists as a homomultimer, coexpression of mutant SARM1 with wild-type SARM1 can act as a dominant-negative, blocking wild-type SARM1 function (Gerdts et al., 2013). SARM1 lacking a TIR domain inhibits wild-type SARM1 function, likely by disrupting the TIR-TIR interactions that activate the enzyme. In addition, we previously identified a highly conserved residue in the TIR do-

<sup>1</sup>Department of Neurology, Washington University School of Medicine in St. Louis, St. Louis, MO; <sup>2</sup>Department of Genetics, Washington University School of Medicine in St. Louis, St. Louis, MO; <sup>3</sup>Department of Developmental Biology, Washington University School of Medicine in St. Louis, St. Louis, MO; <sup>4</sup>Hope Center for Neurological Disorders, Washington University School of Medicine in St. Louis, St. Louis, MO.

Correspondence to Jeffrey Milbrandt: [jmilbrandt@wustl.edu](mailto:jmilbrandt@wustl.edu); Aaron DiAntonio: [diantonio@wustl.edu](mailto:diantonio@wustl.edu).

© 2019 Geisler et al. This article is distributed under the terms of an Attribution-Noncommercial-Share Alike-No Mirror Sites license for the first six months after the publication date (see <http://www.rupress.org/terms/>). After six months it is available under a Creative Commons License (Attribution-Noncommercial-Share Alike 4.0 International license, as described at <https://creativecommons.org/licenses/by-nc-sa/4.0/>).

main that is required for the relief of N-terminal autoinhibition and, hence, injury-induced activation of SARM1 (Summers et al., 2016). Expression of this SARM1 mutant (SARM1-K597E) delays AxD *in vitro* by inhibiting the function of wild-type SARM1. While expressing these SARM1 dominant-negative mutants in wild-type neurons does inhibit pathological AxD, neither blocks axon loss as effectively as the absence of SARM1.

Here we introduced point mutations into human SARM1 and expressed the constructs in wild-type neurons to identify SARM1 dominant-negatives that potently inhibit SARM1 function. We found several SARM1 single mutants that strongly inhibit AxD *in vitro*. Combining the best two of these yields a dominant-negative that potently inhibits SARM1 enzymatic function and protects axons in cellular models of axotomy and neuropathy as robustly as SARM1 KO neurons. Using adeno-associated virus (AAV)-mediated expression of this optimized construct in adult wild-type mice and sciatic nerve cut as a model of severe AxD, we demonstrate axon preservation similar to that observed in SARM1 KO mice. We thus provide a novel strategy to effectively and enduringly inhibit SARM1 function *in vivo*. We anticipate that AAV-mediated expression of SARM1 dominant-negatives could be used therapeutically to block pathological AxD and improve functional outcomes in neuropathies and likely other diseases characterized by acute and chronic AxD. Unlike traditional gene therapy that seeks to treat a single, genetic disorder, gene therapy targeting SARM1 has the potential to treat a wide range of diseases characterized by a shared pathological process—axon loss.

## Results and discussion

### Identification of SARM1 dominant-negative mutants that inhibit AxD

To develop potent SARM1 dominant-negatives, we introduced individual point mutations in highly conserved regions of the N-terminal and TIR domains (Fig. 1 A) and tested if lentivirus-mediated expression of these constructs decreases AxD. All constructs were well expressed in cultured dorsal root ganglion (DRG) neurons (Fig. S1). Axons were severed, and cell bodies were removed to avoid axon regrowth into the injury site. With the aid of high-throughput automated imaging and an automated AxD index (Sasaki et al., 2009), we assessed fragmentation of distal axons over time. Fragmentation of axons begins ~6 h after cut and is complete by 24 h (Fig. 1, B and C). Expression of the previously discovered dominant-negatives SARM1-K597E (Summers et al., 2016) and SARM1-deltaTIR (Gerdt et al., 2013) in wild-type DRG neurons delays AxD until 36 h after axotomy (Fig. 1, B and C). We recently identified glutamic acid E642 as the key catalytic residue within the active site of the TIR NADase (Essuman et al., 2017). To evaluate if blocking enzyme function would yield a potent dominant-negative, we expressed SARM1-E642A in wild-type neurons. Although SARM1-E642A is nonfunctional when expressed in SARM1-KO neurons (Essuman et al., 2017), when SARM1-E642A is expressed in wild-type neurons axon fragmentation proceeds with the same kinetics as in wild-type axons expressing enhanced GFP (EGFP) vector (Fig. 1 B). Hence, the SARM1-E642A mutant is nonfunctional but does not act as a dominant-negative, suggesting that it cannot disrupt TIR-TIR in-

teractions that allow for activation of the wild-type TIR NADase. In contrast, introducing a point mutation at another highly conserved residue in the TIR domain, at position H685 (Fig. 1 A), results in a dominant-negative that potently protects axons for 72 h after axotomy (Fig. 1, B and C). Mutating H685 to either Y or A yields constructs whose dominant-negative efficacy is indistinguishable, suggesting that it is the loss of the H rather than the conversion to any particular amino acid that generates the dominant-negative effect (Fig. S2 A). Therefore, this histidine is likely necessary for the TIR-TIR interaction involved in SARM1 activity. The strongest dominant-negative effect was observed when a lysine at 193 in the N terminus was mutated (Fig. 1 A). This lysine is present within a highly conserved region of the N terminus that we hypothesized could be necessary for injury-induced activation of SARM1. SARM1-K193R expression in wild-type DRGs potently protects axons for 72 h after axotomy (Fig. 1, B and C). As with H685, mutating K193 to either R or A generates constructs whose dominant-negative activity is indistinguishable, suggesting that it is the loss of the lysine that blocks injury-induced activation of SARM1 (Fig. S2 A).

As a second index of neuronal health, we examined the mitochondrial potential in severed axons using the fluorescent mitochondrial membrane indicator tetramethylrhodamine methyl ester (TMRM). Activation of SARM1 causes a drop in mitochondrial membrane potential (Summers et al., 2016), which is indicated by loss of red fluorescence. In wild-type DRG neurons expressing EGFP vector or SARM1-E642A, TMRM fluorescence is no longer observed 24 h after axotomy (Fig. 1 C). In contrast, TMRM-positive mitochondria are preserved in wild-type DRGs expressing the SARM1 dominant-negative mutations and in SARM1-KO DRGs (Fig. 1 C), indicating the morphologically intact severed axons remain metabolically active.

To evaluate whether these SARM1 mutants have prodegenerative function on their own, we expressed either wild-type SARM1 or the SARM1 mutants (Fig. 1 A) in cultured SARM1-KO DRG neurons and assessed AxD after axotomy. Axons of SARM1-KO neurons are completely intact for at least 72 h after axotomy (Fig. 1, D and E), whereas reintroducing enzymatically active wild-type SARM1 promotes rapid AxD after severing (Fig. 1, D and E). In contrast, expression of the dominant-negative mutants and SARM1-E642A in SARM1-KO DRGs does not induce AxD for at least 72 h after transection (Fig. 1, D and E) demonstrating that the evaluated SARM1 mutants do not possess prodegenerative capabilities.

### Combining the SARM1-K193R and H685A mutations blocks wild-type SARM1 enzymatic activity and potently protects from AxD in cellular models of axotomy and neuropathy

Although expression of SARM1-K193R (Fig. 1, B and C) and SARM1-H685A (Fig. S2 A) strongly delays AxD after axotomy, the protection is less robust than deletion of SARM1 (Fig. 1, B and C). We therefore evaluated whether a SARM1 molecule with mutations at both K193 and H685 would result in even more potent dominant-negative activity. We generated a construct with both mutations as well as a third mutation, H194A, and we call this construct the SARM1-compound dominant-negative (SARM1-CDN). Subsequent analysis demonstrated that addition of H194A

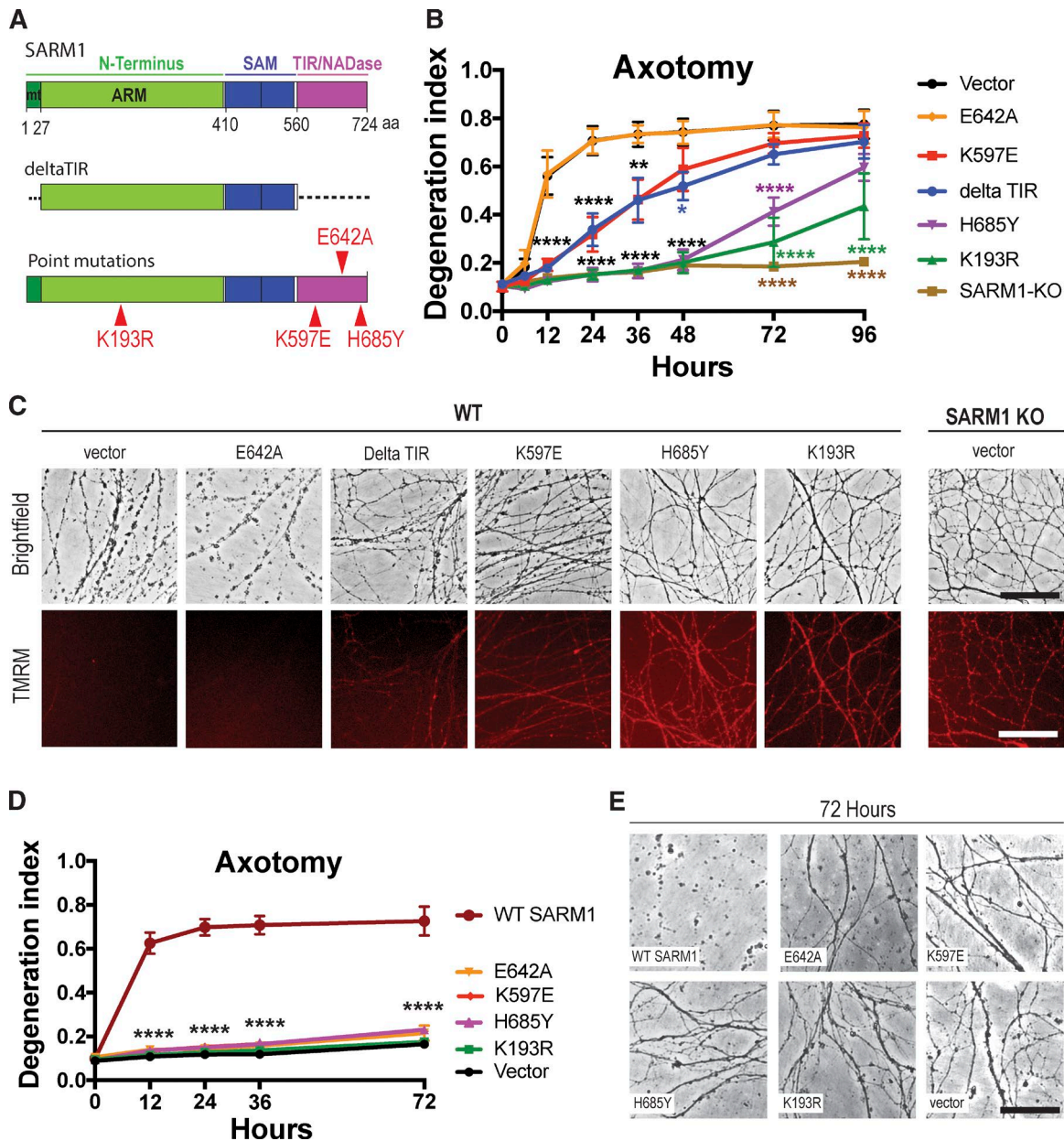


**Figure 1. Identification of SARM1 dominant-negative transgenes.** (A) Schematic representation of the domain structure of human SARM1. Individual point mutations are indicated by red triangles. Dotted segments indicate deleted regions. deltaTIR, aa 1–27 and 560–724 deleted; mt, mitochondrial binding sequence; ARM, HEAT/Armadillo motif; SAM, sterile a motif. (B) Axons of wild-type DRG neurons expressing the indicated constructs or axons of SARM1-KO DRG neurons expressing EGFP vector were transected and imaged using high-throughput automated imaging at indicated time points. AxD was quantified using a DI, which ranges from 0 (perfectly intact) to 1 (perfectly fragmented). Shown are means  $\pm$  SE (SEM) of three independent experiments. Data were tested with a two-way ANOVA showing significant main effects of groups  $F(6,14) = 25.57$ ;  $P < 0.0001$ ; time,  $F(7,98) = 138$ ,  $P < 0.0001$ ; and interaction  $F(42, 98) = 8.809$ ;  $P < 0.0001$ ; post hoc Dunnett’s multiple comparison test; \*\*\*\*,  $P = 0.0001$ ; vector versus deltaTIR, \*\*,  $P = 0.0013$ ; \*,  $P = 0.0122$ ; vector versus K597E, \*\*,  $P = 0.0015$ . (C) Top: Representative brightfield micrographs of wild-type axons expressing indicated constructs or SARM1-KO axons taken 24 h after transection. Bottom: The mitochondrial potential was monitored with red fluorescent TMRM in the same axons as shown in the row above. Upon loss of mitochondrial membrane potential, the red fluorescent signal disappears. (D) Axons of SARM1-KO neurons expressing either enzymatically active, wild-type SARM1 or indicated constructs were transected, and AxD was determined over time. Data are presented as mean  $\pm$  SEM. Two-way ANOVA shows significant main effect of groups  $F(5,12) = 122.5$ ,  $P < 0.0001$ ; time ( $F(4,48) = 124$ ,  $P < 0.001$ ), and interaction  $F(20,48) = 38.94$ ,  $P < 0.0001$ ; Dunnett’s multiple comparison; \*\*\*\*,  $P = 0.0001$ ;  $n = 3$  independent experiments; four wells averaged per experiment. (E) Representative brightfield images of SARM1-KO axons expressing constructs indicated in D, at 72 h after cut. Bars, 50  $\mu$ m (C and E).

does not impact the potency of SARM1-CDN (Fig. S2B); however, since it was generated first and gave such a strong dominant-negative effect, the remainder of our analysis is with SARM1-CDN. Expression of SARM1-CDN completely prevents AxD (Fig. 2, A

and B) and preserves TMRM-positive mitochondria (Fig. 2C) for at least 96 h after axotomy. Upon activation, wild-type SARM1 rapidly degrades  $NAD^+$  (Gerdt et al., 2015; Sasaki et al., 2016; Essuman et al., 2017), which results in local metabolic failure

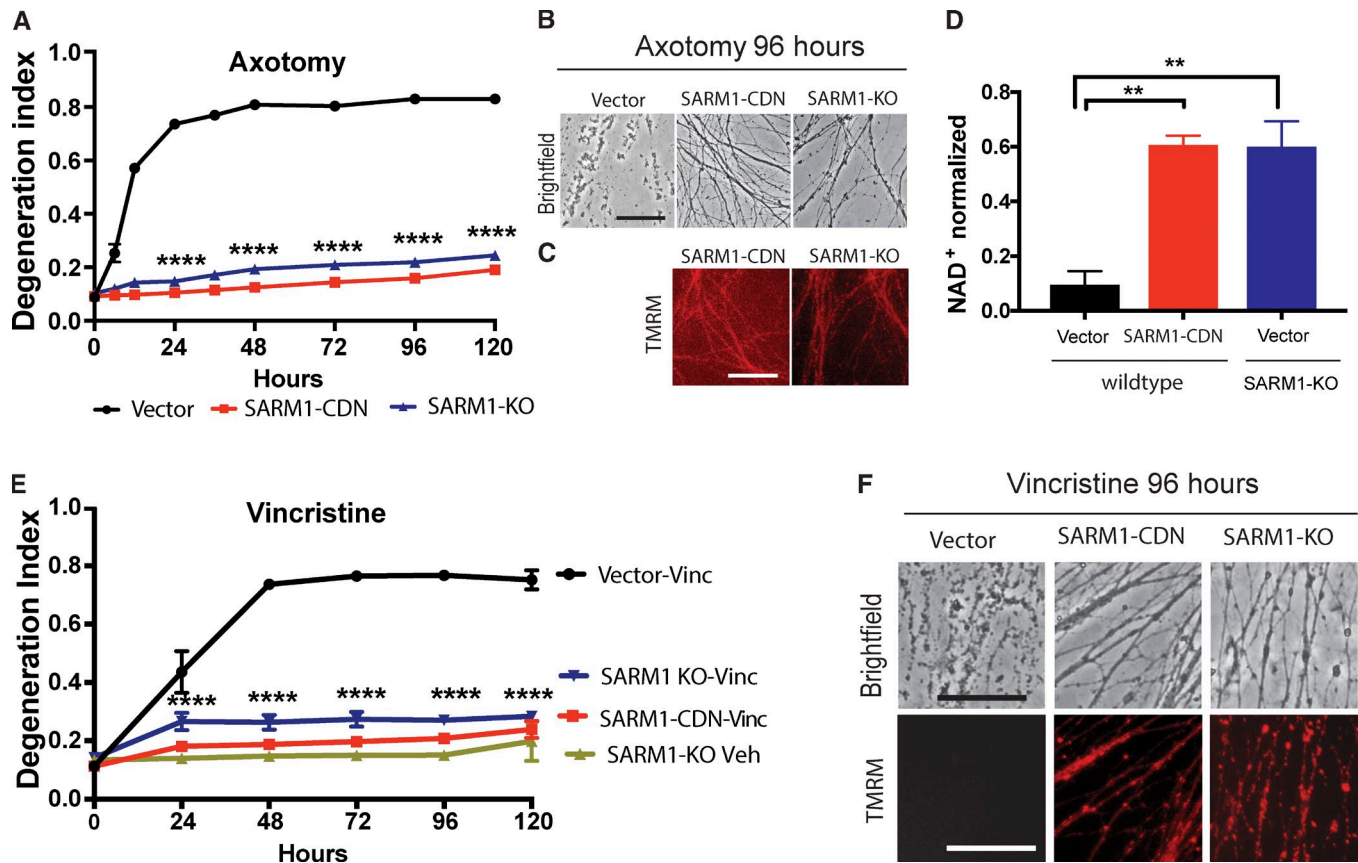


**Figure 2. SARM1-CDN potently inhibits wild-type SARM1 function. (A)** Degeneration of wild-type DRG neurons expressing EGFP vector or the SARM1-CDN and of SARM1 KO neurons expressing EGFP vector after transection. DI ranges from 0 (completely intact) to 1 (completely fragmented). Data are presented as mean  $\pm$  SEM, tested with a two-way ANOVA, which shows significant main effects of group  $F(2,9) = 2,710$ ,  $P < 0.0001$ ; time  $F(8,72) = 298.7$ ,  $P < 0.0001$ , and interaction  $F(16,72) = 154$ ,  $P < 0.0001$ . Dunnett's multiple comparison test vector versus SARM1-CDN and SARM1-KO, \*\*\*\*,  $P = 0.0001$ . **(B and C)** Representative brightfield (B) and TMRM (C) images of axons expressing constructs indicated in A, at 96 h after axotomy. **(D)** HPLC was used to measure NAD<sup>+</sup> levels in wild-type and SARM1-KO neurons expressing EGFP vector or SARM1-CDN from axon extracts 4 h after transection and normalized to baseline (immediately after cut). A one-way ANOVA shows a significant main effect  $F(2,6) = 20.01$ ,  $P = 0.0022$ ; post hoc Tukey's multiple comparison test shows vector versus SARM1-CDN, \*\*,  $P = 0.0036$ ; vector versus SARM1-KO, \*\*,  $P = 0.0039$ ; SARM1-KO versus SARM1-CDN,  $P = 0.9969$ .  $n = 3$  independent experiments. **(E)** Wild-type DRG neurons expressing EGFP vector or SARM1-CDN and SARM1-KO neurons were treated with 40 nM vincristine or vehicle and AxD determined using the DI. Data are represented as means  $\pm$  SEM; two-way ANOVA shows significant main effect of groups  $F(3,8) = 259.6$ ;  $P < 0.0001$ ; time  $F(5,40) = 89.28$ ,  $P < 0.0001$ ; and interaction  $F(15,40) = 38.59$ ;  $P < 0.0001$ ; post hoc Dunnett's multiple comparison test shows wild-type vector vincristine versus SARM1-CDN vincristine, SARM1-KO vincristine, and SARM1-KO vehicle, \*\*\*\*,  $P = 0.0001$ ;  $n = 3$  independent experiments. **(F)** Representative brightfield (top row) and TMRM (bottom row) images of the constructs indicated in D, at 96 h after vincristine administration. Bars, 50  $\mu$ m.

(Gerds et al., 2015; Yang et al., 2015) and subsequent AxD. To assess whether SARM1-CDN also blocks this molecular activity of SARM1, we measured axonal NAD<sup>+</sup> levels in healthy and injured axons. As expected, 4 h after transection, NAD<sup>+</sup> is largely depleted in wild-type neurons expressing a control vector (Fig. 2 D). In contrast, NAD<sup>+</sup> is maintained in wild-type neurons expressing SARM1-CDN and in SARM1-KO neurons (Fig. 2 D). Hence, expression of SARM1-CDN in wild-type neurons potently blocks SARM1 enzymatic function and its prodegenerative activity.

The loss of SARM1 inhibits AxD in models of disease, including traumatic brain injury (Henninger et al., 2016; Ziogas and Koliatsos, 2018) and chemotherapy-induced peripheral neuropathy (Geisler et al., 2016; Turkiew et al., 2017). To examine the effects of SARM1-CDN in chemotherapy-induced peripheral neuropathy, we treated wild-type DRGs with vincristine and observed complete fragmentation of axons 48 h after application of the drug (Fig. 2 E). In contrast, axons of both SARM1-KO neu-

rons as well as wild-type neurons expressing the SARM1 dominant-negative mutant are morphologically intact and retain TMRM-positive mitochondria for at least 96 h after vincristine application (Fig. 2, E and F). Taken together, these data demonstrate that expressing SARM1-CDN in wild-type neurons potently inhibits SARM1 function in response to diverse insults in vitro.

#### SARM1-CDN is strongly expressed in DRG neurons and peripheral nerves upon AAV-mediated gene transfer

We next tested if SARM1-CDN exhibits axoprotective properties in vivo. As a proof of concept, we used sciatic nerve transection as a model of severe pathological AxD, reasoning that this is the most robust test of efficacy. SARM1-CDN fused to EGFP (Fig. 3 A) or EGFP alone were cloned into an AAV8 vector and expressed under the neuron-specific human synapsin (Syn) promoter (Fig. 3 A). 5 wk after intrathecal administration of AAV8-Syn-SARM1-CDN-EGFP (AAV-SARM1-CDN) or con-

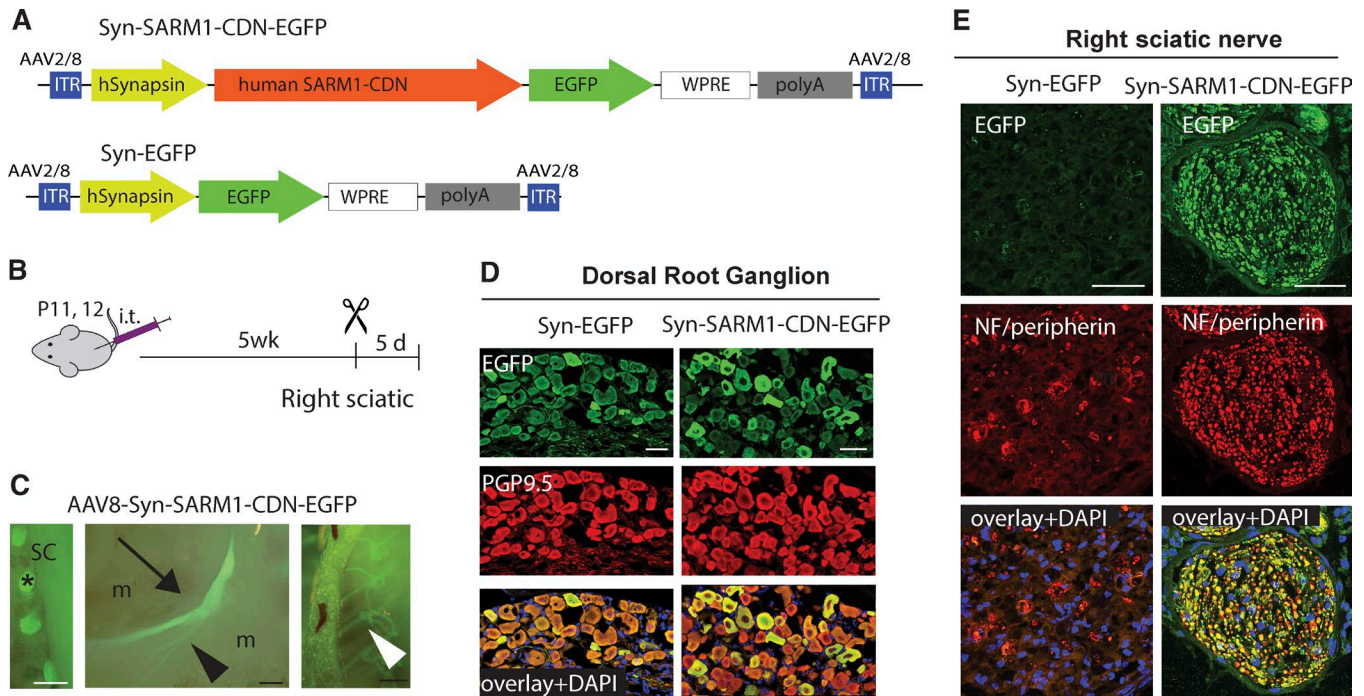


**Figure 3. SARM1-CDN efficiently transduces DRGs in vivo and protects from AxD.** (A) Top: Schematic of the AAV vector expressing human SARM1-CDN under control of the neuron-specific human synapsin promoter (Syn-SARM1-CDN-EGFP). Bottom: Schematic of the EGFP vector (Syn-EGFP) used for control experiments. WPRE, woodchuck hepatitis virus posttranscriptional regulatory element; ITR, inverted terminal repeats. (B) AAV8-Syn-SARM1-CDN-EGFP or EGFP vector (AAV8-Syn-EGFP) were injected intrathecally (i.t.) into mice at postnatal day 11 or 12 (P11/12). 5 wk later, the right sciatic nerve was transected, and 5 d later, tissue was collected for analysis. (C) Representative micrographs taken in situ of (from left to right) DRGs (asterisk) attached to the spinal cord (SC), the left (uninjured) sciatic nerve (arrow) with its branches (arrowheads), and intercostal nerves (white arrowhead) expressing GFP 5.5 wk after injection with AAV8-Syn-SARM1-CDN-EGFP; m, muscle. Bars, 2 mm. (D) Representative confocal image of a 6- $\mu$ m-thick section of a DRG after injecting EGFP vector (left column; Syn-EGFP) or SARM1-CDN (right column; Syn-SARM1-CDN-EGFP). Sections were stained with PGP9.5 (red; DRG neurons) and anti-GFP (green; construct expression) and coverslipped with Vectamount containing DAPI (blue; nuclear marker). (E) Representative confocal image of a 6- $\mu$ m-thick section of the right (transected) sciatic nerve taken 5 d after cut in mice injected with the EGFP vector (left column; Syn-EGFP) or SARM1-CDN (right column; Syn-SARM1-CDN-EGFP). Sections were stained with antibodies to Neurofilament 200 (NF) and peripherin (red; axonal markers) and green fluorescent protein (green; construct expression) and mounted with Vectashield containing DAPI (blue; nuclear marker). Bars, 50  $\mu$ m (D and E).

control EGFP virus (Fig. 3 B) we observed robust EGFP labeling of DRGs and peripheral nerves, including the sciatic (Fig. 3, C and E) and intercostal nerves (Fig. 3 C). DRGs are efficiently transduced as determined by staining with the neuronal marker PGP9.5 (Fig. 3 D).

Before evaluating the role of the SARM1-CDN in blocking injury-induced AxD, we first assessed whether expression of AAV-SARM1-CDN induces morphological changes to axons in the absence of injury. Axons of sciatic nerves of mice injected with AAV-SARM1-CDN and AAV-EGFP appeared morphologically intact with no significant difference in axon size distribution and G ratio (Fig. S3). Hence, expression of SARM1-CDN has no detectable influence on axons in the absence of injury.

### SARM1-CDN potently protects from AxD in vivo

5 d after sciatic transection, axons are largely absent in the distal nerve segment in mice injected with control virus, as evidenced by lack of EGFP fluorescence and loss of neurofilament and peripherin staining (Fig. 3 E). In contrast, EGFP fluorescence and neurofilament and peripherin staining are readily observed in nerves of mice injected with AAV-SARM1-CDN (Fig. 3 E), indicating that axons expressing the dominant-negative are protected from degeneration.

The severity of axonal loss after nerve cut and degree of protection afforded by the dominant-negative are even better appreciated using plastic-embedded thin sections. 5 d after transection, signs of widespread Wallerian degeneration, including Schwann cells with myelin debris, lipid-laden histiocytes, and axon remnants with dark cytoplasm (Fig. 4, A, A', C, and C'), are apparent in cross sections of the sural nerve, a sensory branch of the sciatic nerve distal to the cut. In contrast, in mice injected with AAV-SARM1-CDN, myelinated axons are remarkably well preserved, with normal shape, myelin thickness, and internal architecture (Fig. 4, B, B', D, and D'). With the aid of electron microscopy, it becomes evident that this protection also extends to unmyelinated axons (Fig. 4, D and D'). When we compared numbers of myelinated axons on the injured and uninjured sides, mice injected with EGFP vector show a reduction of ~99% (ipsilateral  $5 \pm 0.9$  axons/nerve; contralateral  $446 \pm 57$  axons/nerve;  $n = 4$  mice; Fig. 4 E), whereas there is no significant axon loss in mice expressing SARM1-CDN (cut site,  $389 \pm 13$  axons/nerve; contralateral  $396 \pm 28$  axons,  $n = 5$  mice; Fig. 4 E) or in SARM1-KO mice (Fig. 4 E). Even 10 d after transection, distal axons are present in mice injected with SARM1-CDN (Fig. 4 G). While we did not detect axons in the sural nerves of the vector treated group at that time point ( $0.3 \pm 0.3$  axons;  $n = 3$  mice; Fig. 4, F and G),

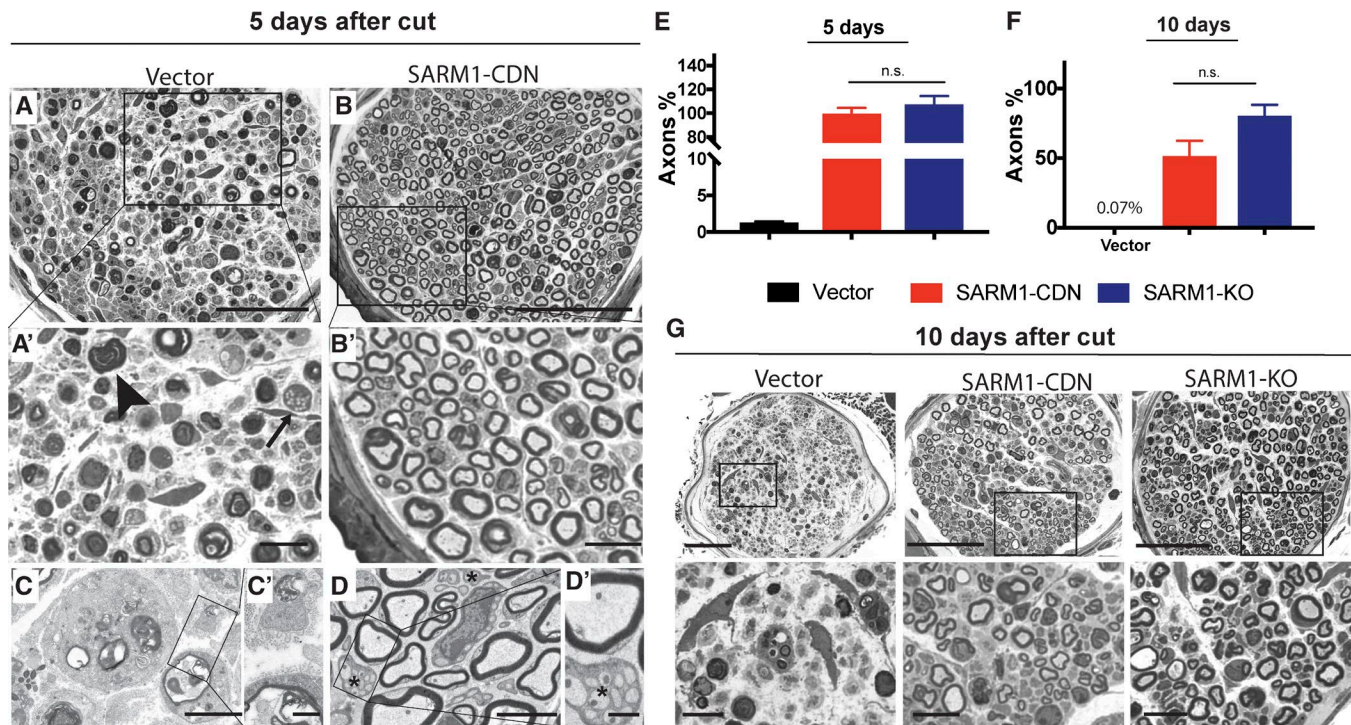


**Figure 4. SARM1-CDN protects from AxD in vivo with efficacy similar to SARM1-KO. (A and B)** Representative photomicrographs of toluidine blue–stained semithin cross sections of the right sural nerve 5 d after transection of the sciatic nerve in mice injected with vector (A;  $n = 4$ ) or SARM1-CDN (B;  $n = 5$ ). A' and B' show enlargements of areas indicated by rectangles in A and B. The arrow and arrowhead indicate lipid-laden histiocytes and myelin debris, respectively. **(C and D)** Representative electron micrographs of the right sural nerve of a mouse injected with EGFP vector showing complete loss of internal nerve architecture (C) whereas unmyelinated (asterisks) and myelinated axons are preserved after SARM1-CDN injection (D). C' and D' show enlargements of areas indicated by rectangles in C and D. **(E and F)** All axons in cross sections of the entire sural nerve were counted in wild-type mice injected with vector ( $n = 4$  in E;  $n = 3$  in F) or SARM1-CDN ( $n = 5$  in E,  $n = 3$  in F) or in SARM1-KO mice ( $n = 5$  in E and F) and expressed as percentage of axon numbers of the respective intact contralateral sides at 5 (E) and 10 (F) d after transection. Data are presented as mean  $\pm$  SE (SEM), tested with a one-way ANOVA, which shows significant main effects in E ( $F(2,11) = 97.13$ ,  $P < 0.0001$ ; post hoc Tukey's multiple comparison test shows vector versus SARM1-SARM1-CDN, \*\*\*\*,  $P < 0.0001$ ; vector versus SARM1-KO, \*\*\*\*,  $P < 0.0001$ ; SARM1-CDN versus SARM1-KO,  $P = 0.5953$ ) and F ( $F(2,8) = 20.73$ ;  $P = 0.0007$ ; Tukey's multiple comparison test shows vector versus SARM1-CDN, \*\*,  $P = 0.0077$ ; vector versus SARM1-KO, \*\*\*,  $P = 0.0005$ ; SARM1-CDN versus SARM1-KO,  $P = 0.2543$ ). n.s., not significant. **(G)** Representative micrographs of toluidine blue–stained sections of the sural nerve 10 d after cut. Bottom row displays enlargements of indicated areas in the images above. Bars, 50  $\mu$ m (A and B), 10  $\mu$ m (A' and B'), 5  $\mu$ m (C and D), 1  $\mu$ m (C' and D'), 50  $\mu$ m (G, top), and 10  $\mu$ m (G, bottom).

we identified  $160 \pm 40$  axons per sural nerve ( $n = 3$  mice) in the AAV-SARM1-CDN group, which is  $\sim 59 \pm 15\%$  of the number of axons present in the uninjured nerve (Fig. 4 F). This preservation is comparable to SARM1-KO mice (Fig. 4, F and G), in which  $79 \pm 9\%$  of axons remain distal to injury site (Fig. 4, F and G).

### Concluding remarks

In this study, we establish AAV-mediated, neuron-specific expression of a SARM1 dominant-negative as a powerful tool to potently inhibit AxD in vivo. These findings demonstrate that SARM1 acts neuron-autonomously and show that it can be effectively targeted in adult wild-type mice. Our findings translate the recent dramatic progress in defining the molecular mechanism of axon degeneration into a novel therapeutic strategy to block pathological AxD in neurological disorders.

SARM1 is a multimer, and mutant SARM1 coassembles with wild-type SARM1 (Gerdt et al., 2013). Hence, the relative dominant-negative efficacy of distinct SARM1 mutants may give mechanistic clues to SARM1 function, although differences in expression and/or localization may also contribute. Mutating residues K193 or H685 in SARM1 generates very potent domi-

nant-negative transgenes, indicating that K193 in the N terminus and H685 in the TIR domain are likely essential for activation of SARM1. Interestingly, mutating the active site of the TIR domain (E642A) completely abrogates SARM1 function when reexpressed in SARM1 null neurons, but has no dominant-negative effect when expressed in wild-type neurons. This suggests that each enzymatic active site in the complex functions independently. However, our data (Gerdt et al., 2013) as well as a vast literature on other TIR domain proteins (Narayanan and Park, 2015) demonstrate that TIR dimer interactions are necessary for activation of TIR domains. We suggest that while the E642 residue is necessary for intrinsic enzymatic activity of a TIR domain, the H685 residue is necessary for activation of enzyme activity in the adjacent, interacting TIR domain, and so when mutated can act as a dominant-negative. In addition, N-terminal residues such as K193 appear to be required for injury-induced activation of SARM1 via relief of autoinhibitory interactions with the TIR domain. Because the effects of H685A and K193R mutations are additive, their mechanisms of inhibition are likely distinct.

Many common neurodegenerative diseases are characterized by early AxD (Burke and O'Malley, 2013; Howell et al., 2013;

Johnson et al., 2013; Yin et al., 2016). Peripheral neuropathies are the most common neurodegenerative diseases, affecting >20 million people in the US alone. Many neuropathies are caused by degeneration of long axons, yet specific therapies to block this degeneration do not exist. Furthermore, in some of the most prevalent diseases of the central nervous system, such as Parkinson's disease, traumatic brain injury, and glaucoma, AxD precedes neuronal degeneration (Tagliaferro and Burke, 2016; Caminiti et al., 2017; Fazio et al., 2018; O'Keeffe and Sullivan, 2018). Studies using *Wallerian degeneration slow (wld<sup>s</sup>)* mice, which harbor a spontaneous mutation that delays AxD (Lunn et al., 1989), and SARM1-KO mice demonstrate that inhibiting the axon destruction program leads to greatly improved functional outcomes (Wang et al., 2001, 2002; Sajadi et al., 2004; Meyer zu Horste et al., 2011; Geisler et al., 2016; Henninger et al., 2016; Fernandes et al., 2018). The active component of WLD<sup>s</sup> fusion protein is NMNAT1 (Araki et al., 2004), which inhibits SARM1 (Gilley et al., 2015; Sasaki et al., 2016). However, expression of WLD<sup>s</sup> is less effective than genetic deletion of SARM1 in protecting axons of older mice and in preserving synapses (Conforti et al., 2014; Gilley et al., 2017), suggesting that directly targeting SARM1 will provide better inhibition of pathological AxD. Here we demonstrate that viral delivery of SARM1-CDN in mice induces long-lasting axon protection following sciatic nerve transection, the most rapid and aggressive trigger of AxD, providing a template for gene therapy treatments of slower axon loss in chronic neurodegenerative diseases.

AAV-mediated gene delivery has been safely used in patients in clinical trials and has shown promising results in neurological diseases, e.g., spinal muscular atrophy (Mendell et al., 2017; Sumner and Crawford, 2018). AAV effectively transduces neurons, is not pathogenic, and supports long-lasting expression after a single delivery (Hwu et al., 2012; Mittermeyer et al., 2012). Thus, AAV-mediated expression of SARM1-CDN, if proven safe in humans, may be useful for the treatment of chronic neurodegenerative diseases, such as hereditary and idiopathic neuropathies and Parkinson's disease, as well as acquired neuropathies, such as chemotherapy-induced neuropathy. In treating chemotherapy-induced neuropathy, it is tempting to speculate that a single injection of AAV-SARM1-CDN may be sufficient to provide axon protection for the duration of chemotherapy treatment.

## Materials and methods

All procedures were performed in accordance with guidelines mandated in the National Institutes of Health Guide for the Care and Use of Laboratory Animals and approved by the Washington University School of Medicine in St. Louis Institutional Animal Care and Use Committee (protocols 20170030 and 20150043). This manuscript was prepared in adherence to the ARRIVE guidelines. Pregnant C57Bl/6NTac mice were purchased from Taconic and pregnant CD1 mice were purchased from Charles River. SARM1 KO mice were a gift from Marco Colonna (Department of Pathology and Immunology, Washington University School of Medicine in St. Louis, St. Louis, MO; Szretter et al., 2009) and bred in our colony. Male and female mice were used for all experiments. Chemicals were purchased from Sigma-Aldrich unless indicated otherwise.

## DRG culture

DRGs were dissected from embryonic day 13.5 (E13.5) or E14.5 CD-1 (Charles River) or from E13.5 SARM1 KO mouse embryos in Dulbecco's modified Eagle's medium. DRG neurons were dissociated in 0.05% trypsin-EDTA at 37°C, resuspended in Neurobasal media (Invitrogen) containing 2% B27 (Invitrogen), 50 ng/ml nerve growth factor (Harlan Laboratories), 1 μM 5-fluoro-2-deoxyuridine, and 1 μM uridine and plated in 48-well plates coated with poly-D-lysine and laminin. Concentrated lentivirus was added at 50-fold final dilution the following day (DIV1). All experiments with direct comparisons were performed on the same plate to minimize variability.

## Lentiviral constructs and infection

Mammalian expression constructs were derived from an FCIV lentiviral vector (Araki et al., 2004) containing a ubiquitin promoter and Venus marker. Venus-tagged SARM1 fusion proteins were created by inserting SARM1 cDNA in frame with Venus with an Ala-Thr-Thr linker between the SARM1 C terminus and Venus. SARM1 mutant constructs were generated by the megaprimer PCR method. The SARM1 deletion mutant lacking residues 2–27 and 561–724 (deltaTIR) was subcloned into FCIV using the InFusion system. The control vector contained Venus or EGFP under control of the ubiquitin promoter (EGFP vector). Successful insertions of clones were verified by sequencing. Lentiviral particles were produced by cotransfection of the lentiviral expression vector FCIV with lentiviral packaging plasmid psPAX2 and vesicular stomatitis virus glycoprotein into HEK293T cells as described previously (Araki et al., 2004). Lentiviral particles were collected 48 h after transfection and concentrated with Lenti-X concentrator (Clontech) to a final concentration of 1–10 × 10<sup>7</sup> infectious particles/ml. Lentiviral expression of constructs was confirmed by positive fluorescence signal in the cell bodies and ranged from 92.2 ± 7.6% (SARM1-delta TIR) to 98.8 ± 0.7% (SARM1-E642A; Fig. S1) infected DRGs.

## Axotomy and vincristine

DRG neurons were cultured in 48-well microtiter plates with cell bodies sequestered to allow imaging of axons by automated microscopy. On DIV8, axons of DRGs were severed manually near the somae with a 3-mm-wide flat blade under microscopic guidance. Cell bodies were removed to preclude axon regeneration. Vincristine (40 nM in DMSO) or vehicle (DMSO) was added on DIV8 and remained in the wells until the end of the experiment.

## Imaging and quantification of AxD

15–20 brightfield images per well of live axons were acquired at indicated time points using an Operetta high-content imaging system (PerkinElmer) with a 20× objective. Axon degeneration was quantified based on axon morphology and reported as the “degeneration index” (DI) using an ImageJ-based script (Sasaki et al., 2009); DI ranges from 0 (perfectly intact) to 1 (perfectly fragmented). Values >0.5 indicate extensive axon degeneration. All images were inspected, and fields without axons or inadequate imaging were omitted. 10–15 images per well were measured as technical replicates. All experiments were performed at least three times, and three to five wells per condition were averaged.

for each experiment. To assess mitochondrial potential, TMRM (Thermo Fisher Scientific) was added, and axons were imaged 30 min later with an inverted Olympus CKX41 microscope and Nikon DS-QiLMC camera. Exposure times were kept constant between constructs. Brightfield images were obtained in phase contrast using the same microscope and camera.

#### HPLC quantification of NAD<sup>+</sup>

CD1 E13.5 DRGs and SARM1 KO E13.5 DRGs were plated as spot cultures in 24-well plates coated with poly-D-lysine and laminin. On DIV1, neurons were transduced with concentrated virus expressing either Ubiquitin-EGFP or Ubiquitin-SARM1-CDN-Venus. On DIV6, axons were severed, and cell bodies were removed as described. Immediately (0 h time point) or 4 h after axotomy, axons were washed with cold 0.9% saline and lysed by addition of 0.5 M perchloric acid. Extracts were centrifuged, and supernatants were collected, neutralized with 3 M K<sub>2</sub>CO<sub>3</sub>, and diluted in potassium phosphate buffer. NAD<sup>+</sup> was assayed by HPLC on an LC-18T HPLC column (Supelco) at a flow rate of 1 ml/min. Elution peaks were matched to NAD<sup>+</sup> standards. Four wells per condition were averaged, and three independent experiments were performed.

#### AAV constructs and virus injections

AAV vector expressing EGFP under control of the human synapsin promoter was obtained from Addgene (gift from Bryan Roth, School of Medicine at the University of North Carolina at Chapel Hill, NC; Addgene #50465) and used as EGFP vector control (Addgene viral prep #50465-AAV8). pAAV-hSyn-EGFP (Addgene #50465) was cut with BamHI and NcoI, and SARM1-K193R/H194A/H685A (SARM1-CDN) was inserted between the synapsin promoter and EGFP sequence using inFusion (Clontech) system. AAV8-hSyn-SARM1-CDN-EGFP was generated by the viral vector core of the Hope Center for Neurological Disorders at Washington University in St. Louis. Viral particles were purified by iodixanol gradient ultracentrifugation, and virus titers were measured by dot blot. Under light anesthesia with Avertin,  $6 \times 10^{11}$  viral genomes were injected intrathecally at L6/S1 into male ( $n = 7$ ) and female ( $n = 10$ ) C57Bl/6 mice (Taconic) at postnatal day 11 or 12. Two female mice injected with EGFP vector died subsequently, whereas none injected with the SARM1 dominant-negative construct died.

#### Sciatic nerve transection and tissue collection

5 wk after virus injection, one group of mice ( $n = 9$ ) was anesthetized with isoflurane, the right sciatic nerve transected and nerve ends bent away from each other to prevent reconnection. 5 d after nerve transection, mice were anesthetized with Avertin and, after the sciatic and sural nerves were dissected out, perfused transcardially with 4% paraformaldehyde in phosphate buffered saline. Spinal cord and DRGs were dissected out, cryoprotected overnight in 30% sucrose, and frozen in Tissue-Tek optimal cutting temperature compound (Electron Microscopy Sciences) in liquid 2-methylbutane cooled by dry ice. The sciatic nerves of a second group of mice ( $n = 6$ ) were transected 8 wk after virus injection, and tissue was collected 10 d later as described above. For comparison, age-matched (11 wk) SARM1 KO mice ( $n = 10$ ;

5 male/5 female) received a sciatic nerve transection, and sciatic and sural nerves were dissected out 5 ( $n = 5$  mice; 2 female/3 male) or 10 ( $n = 5$  mice, 3 female/2 male) d after transection.

#### Toluidine blue staining and axon quantification

Sural and sciatic nerves were fixed over night by immersion in freshly prepared 3% glutaraldehyde in 0.1 M PBS and processed as described recently (Geisler et al., 2016). Cross sections (400 nm thick) were cut using a Leica EM UC7 ultramicrotome and stained with 1% toluidine blue (Fisher Scientific). Sural nerve sections were imaged with the 63 $\times$  oil immersion objective of a Leica DMI 4000B microscope equipped with a Leica DFC 7000-T Camera. Micrographs were stitched using the Leica software, and all axons per cross section were counted in ImageJ. To determine axon size distribution and G ratios of the sciatic nerve, four non-overlapping areas per cross section were imaged with a 100 $\times$  oil objective of a Zeiss Axioskop and photographed with a Hitachi camera. Photographs were analyzed with a customized semiautomated binary imaging analysis method (Hunter et al., 2007). Three nerves per treatment group were analyzed, and results of four areas per nerve were averaged. All analyses were done by blinded observers.

#### Electron microscopy

Selected blocks of sural nerves were used to cut 90-nm-thick ultrathin sections, which were stained with uranyl acetate and lead citrate and viewed with a JEOL JEM 1400 TEM.

#### Immunohistochemistry

6- $\mu$ m-thick sections of DRGs and sciatic nerves were cut at the cryostat (Leica CM1860), mounted onto slides, and processed as described recently (Geisler et al., 2016). Experiments with direct comparisons between groups were performed in parallel to minimize variability. Primary antibodies included rabbit anti-Protein Gene Product 9.5 (1:1,000; EMD Millipore; #AB1761-1-I), rabbit anti-peripherin (1:250; EMD Millipore; #AB1530), rabbit anti-neurofilament 200 (1:1,000, Sigma-Aldrich; #N4142), and mouse-anti-GFP conjugated to Alexa Fluor 488 (1:250; Thermo Fisher Scientific; #A-21311). Secondary antibody was Alexa Fluor 594-conjugated goat anti-rabbit (Invitrogen) at a dilution of 1:500. Sections were coverslipped with Vectashield with DAPI (Vector Laboratories) to allow visualization of nuclei. Sciatic nerves and DRGs were imaged with the confocal mode of the Leica DMI 4000B using 40 $\times$  and 20 $\times$  immersion oil objectives, respectively. PGP9.5-positive and GFP-positive DRG neurons were counted in one stitched confocal slice of the entire DRG in ImageJ. One section each of two different DRGs was counted per animal, and values were averaged. GFP was expressed in  $85 \pm 0.4\%$  of PGP9.5-positive DRG neurons after injection of AAV8-Syn-SARM1-CDN-EGFP.

#### Statistical analysis

Unless otherwise stated, data are reported as means  $\pm$  SEM. Between-group comparisons were made with one-way or two-way ANOVA as appropriate. Two-sided significance tests were used throughout, and  $P < 0.05$  was considered statistically significant. All statistics were calculated with the aid of Prism software.



## Online supplemental material

Fig. S1 depicts photomicrographs showing expression of SARM1 dominant-negative-Venus constructs in DRG neurons and associated quantification confirming that all constructs are well expressed. Fig. S2 depicts graphs comparing different SARM1 dominant-negative constructs demonstrating no difference in axon protection between SARM1-H685A and SARM1-H685Y and between SARM1-K193R and SARM1-K193A, as well as between SARM1-K193R/H685A and SARM1-K193R/H194A/H685A. Fig. S3 depicts representative photomicrographs of toluidine blue-stained semithin cross sections of the sciatic nerve following injections of EGFP vector (AAV-Syn-EGFP) and the SARM1 dominant-negative (AAV-Syn-SARM1-CDN-EGFP) and associated analysis of axon size distribution and G ratios, revealing no significant difference between nerves from mice injected with EGFP vector and the SARM1 dominant-negative.

## Acknowledgments

We thank Kelli Simburger and Tim Fahrner for cloning of the constructs and Rachel McClamey for assistance cutting semithin sections.

This work was supported by National Institutes of Health grants K08NS091448 (S. Geisler), R01CA219866, R01NS087632, and R01CA218263 (J. Milbrandt and A. DiAntonio); Muscular Dystrophy Association grant MDA344513 (D.W. Summers); the Thompson Family Foundation Initiative grant PDS 155352 (S. Geisler, A. DiAntonio, and J. Milbrandt); and the Hope Center Viral Vector Core at Washington University School of Medicine in St. Louis.

S. Geisler, D.W. Summers, X. Mao, A. DiAntonio, J. Milbrandt, and Washington University are inventors on patents related to this work. A. DiAntonio and J. Milbrandt are cofounders of Disarm Therapeutics and members of its scientific advisory board. The authors declare no additional competing financial interests.

Author contributions: Experimental design, S. Geisler, J. Milbrandt, and A. DiAntonio; Investigation, S. Geisler, S.X. Huang, A. Strickland, R.A. Doan, D.W. Summers, X. Mao, and J. Park; Formal analysis, S. Geisler, S.X. Huang, and R.A. Doan; Writing (original draft), S. Geisler; Writing (review and editing), S. Geisler, A. DiAntonio, and J. Milbrandt; Funding acquisition, S. Geisler, D.W. Summers, A. DiAntonio, and J. Milbrandt; Resources, S. Geisler, A. DiAntonio, and J. Milbrandt; Supervision, S. Geisler, A. DiAntonio, and J. Milbrandt.

Submitted: 2 June 2018

Revised: 22 August 2018

Accepted: 13 December 2018

## References

Araki, T., Y. Sasaki, and J. Milbrandt. 2004. Increased nuclear NAD biosynthesis and SIRT1 activation prevent axonal degeneration. *Science*. 305:1010–1013. <https://doi.org/10.1126/science.1098014>

Burke, R.E., and K. O'Malley. 2013. Axon degeneration in Parkinson's disease. *Exp. Neurol.* 246:72–83. <https://doi.org/10.1016/j.expneurol.2012.01.011>

Caminiti, S.P., L. Presotto, D. Baroncini, V. Garibotto, R.M. Moresco, L. Gianolli, M.A. Volonté, A. Antonini, and D. Perani. 2017. Axonal damage and loss of connectivity in nigrostriatal and mesolimbic dopamine pathways in early Parkinson's disease. *Neuroimage Clin.* 14:734–740. <https://doi.org/10.1016/j.nicl.2017.03.011>

Cashman, C.R., and A. Höke. 2015. Mechanisms of distal axonal degeneration in peripheral neuropathies. *Neurosci. Lett.* 596:33–50. <https://doi.org/10.1016/j.neulet.2015.01.048>

Conforti, L., J. Gilley, and M.P. Coleman. 2014. Wallerian degeneration: an emerging axon death pathway linking injury and disease. *Nat. Rev. Neurosci.* 15:394–409. <https://doi.org/10.1038/nrn3680>

Essuman, K., D.W. Summers, Y. Sasaki, X. Mao, A. DiAntonio, and J. Milbrandt. 2017. The SARM1 Toll/Interleukin-1 Receptor Domain Possesses Intrinsic NAD<sup>+</sup> Cleavage Activity that Promotes Pathological Axonal Degeneration. *Neuron*. 93:1334–1343.e5. <https://doi.org/10.1016/j.neuron.2017.02.022>

Fazio, P., P. Svenningsson, Z. Cselényi, C. Halldin, L. Farde, and A. Varrone. 2018. Nigrostriatal dopamine transporter availability in early Parkinson's disease. *Mov. Disord.* 33:592–599. <https://doi.org/10.1002/mds.27316>

Fernandes, K.A., K.L. Mitchell, A. Patel, O.J. Marola, P. Shrager, D.J. Zack, R.T. Libby, and D.S. Welsbie. 2018. Role of SARM1 and DR6 in retinal ganglion cell axonal and somal degeneration following axonal injury. *Exp. Eye Res.* 171:54–61. <https://doi.org/10.1016/j.exer.2018.03.007>

Geisler, S., R.A. Doan, A. Strickland, X. Huang, J. Milbrandt, and A. DiAntonio. 2016. Prevention of vincristine-induced peripheral neuropathy by genetic deletion of SARM1 in mice. *Brain*. 139:3092–3108. <https://doi.org/10.1093/brain/aww251>

Gerds, J., D.W. Summers, Y. Sasaki, A. DiAntonio, and J. Milbrandt. 2013. Sarm1-mediated axon degeneration requires both SAM and TIR interactions. *J. Neurosci.* 33:13569–13580. <https://doi.org/10.1523/JNEUROSCI.1197-13.2013>

Gerds, J., E.J. Brace, Y. Sasaki, A. DiAntonio, and J. Milbrandt. 2015. SARM1 activation triggers axon degeneration locally via NAD<sup>+</sup> destruction. *Science*. 348:453–457. <https://doi.org/10.1126/science.1258366>

Gerds, J., D.W. Summers, J. Milbrandt, and A. DiAntonio. 2016. Axon Self-Destruction: New Links among SARM1, MAPKs, and NAD<sup>+</sup> Metabolism. *Neuron*. 89:449–460. <https://doi.org/10.1016/j.neuron.2015.12.023>

Gilley, J., G. Orsomando, I. Nascimento-Ferreira, and M.P. Coleman. 2015. Absence of SARM1 rescues development and survival of NMNAT2-deficient axons. *Cell Reports*. 10:1974–1981. <https://doi.org/10.1016/j.celrep.2015.02.060>

Gilley, J., R.R. Ribchester, and M.P. Coleman. 2017. Sarm1 Deletion, but Not Wld<sup>s</sup>, Confers Lifelong Rescue in a Mouse Model of Severe Axonopathy. *Cell Reports*. 21:10–16. <https://doi.org/10.1016/j.celrep.2017.09.027>

Henninger, N., J. Bouley, E.M. Sikoglu, J. An, C.M. Moore, J.A. King, R. Bowser, M.R. Freeman, and R.H. Brown Jr. 2016. Attenuated traumatic axonal injury and improved functional outcome after traumatic brain injury in mice lacking Sarm1. *Brain*. 139:1094–1105. <https://doi.org/10.1093/brain/aww001>

Howell, G.R., I. Soto, R.T. Libby, and S.W.M. John. 2013. Intrinsic axonal degeneration pathways are critical for glaucomatous damage. *Exp. Neurol.* 246:54–61. <https://doi.org/10.1016/j.expneurol.2012.01.014>

Hunter, D.A., A. Moradzadeh, E.L. Whitlock, M.J. Brenner, T.M. Myckatyn, C.H. Wei, T.H.H. Tung, and S.E. Mackinnon. 2007. Binary imaging analysis for comprehensive quantitative histomorphometry of peripheral nerve. *J. Neurosci. Methods*. 166:116–124. <https://doi.org/10.1016/j.jneumeth.2007.06.018>

Hwu, W.-L., S. Muramatsu, S.-H. Tseng, K.-Y. Tzen, N.-C. Lee, Y.-H. Chien, R.O. Snyder, B.J. Byrne, C.-H. Tai, and R.-M. Wu. 2012. Gene therapy for aromatic L-amino acid decarboxylase deficiency. *Sci. Transl. Med.* 4:134ra61. <https://doi.org/10.1126/scitranslmed.3003640>

Johnson, V.E., W. Stewart, and D.H. Smith. 2013. Axonal pathology in traumatic brain injury. *Exp. Neurol.* 246:35–43. <https://doi.org/10.1016/j.expneurol.2012.01.013>

Lunn, E.R., V.H. Perry, M.C. Brown, H. Rosen, and S. Gordon. 1989. Absence of Wallerian Degeneration does not Hinder Regeneration in Peripheral Nerve. *Eur. J. Neurosci.* 1:27–33. <https://doi.org/10.1111/j.1460-9568.1989.tb00771.x>

Mendell, J.R., S. Al-Zaidy, R. Shell, W.D. Arnold, L.R. Rodino-Klapac, T.W. Prior, L. Lowes, L. Alfano, K. Berry, K. Church, et al. 2017. Single-Dose Gene-Replacement Therapy for Spinal Muscular Atrophy. *N. Engl. J. Med.* 377:1713–1722. <https://doi.org/10.1056/NEJMoa1706198>

Meyer zu Horste, G., T.A. Miesbach, J.I. Muller, R. Fledrich, R.M. Stassart, B.C. Kieseier, M.P. Coleman, and M.W. Sereda. 2011. The Wlds transgene

- reduces axon loss in a Charcot-Marie-Tooth disease 1A rat model and nicotinamide delays post-traumatic axonal degeneration. *Neurobiol. Dis.* 42:1–8. <https://doi.org/10.1016/j.nbd.2010.12.006>
- Mittermeyer, G., C.W. Christine, K.H. Rosenbluth, S.L. Baker, P. Starr, P. Larson, P.L. Kaplan, J. Forsayeth, M.J. Aminoff, and K.S. Bankiewicz. 2012. Long-term evaluation of a phase 1 study of AADC gene therapy for Parkinson's disease. *Hum. Gene Ther.* 23:377–381. <https://doi.org/10.1089/hum.2011.220>
- Narayanan, K.B., and H.H. Park. 2015. Toll/interleukin-1 receptor (TIR) domain-mediated cellular signaling pathways. *Apoptosis.* 20:196–209. <https://doi.org/10.1007/s10495-014-1073-1>
- O'Keefe, G.W., and A.M. Sullivan. 2018. Evidence for dopaminergic axonal degeneration as an early pathological process in Parkinson's disease. *Parkinsonism Relat. Disord.* 56:9–15. <https://doi.org/10.1016/j.parkreldis.2018.06.025>
- Osterloh, J.M., J. Yang, T.M. Rooney, A.N. Fox, R. Adalbert, E.H. Powell, A.E. Sheehan, M.A. Avery, R. Hackett, M.A. Logan, et al. 2012. dSarm/Sarm1 is required for activation of an injury-induced axon death pathway. *Science.* 337:481–484. <https://doi.org/10.1126/science.1223899>
- Sajadi, A., B.L. Schneider, and P. Aebischer. 2004. Wlds-mediated protection of dopaminergic fibers in an animal model of Parkinson disease. *Curr. Biol.* 14:326–330. <https://doi.org/10.1016/j.cub.2004.01.053>
- Sasaki, Y., B.P.S. Vohra, F.E. Lund, and J. Milbrandt. 2009. Nicotinamide mononucleotide adenylyl transferase-mediated axonal protection requires enzymatic activity but not increased levels of neuronal nicotinamide adenine dinucleotide. *J. Neurosci.* 29:5525–5535. <https://doi.org/10.1523/JNEUROSCI.5469-08.2009>
- Sasaki, Y., T. Nakagawa, X. Mao, A. DiAntonio, and J. Milbrandt. 2016. NMN AT1 inhibits axon degeneration via blockade of SARM1-mediated NAD<sup>+</sup> depletion. *eLife.* 5:e19749. <https://doi.org/10.7554/eLife.19749>
- Summers, D.W., D.A. Gibson, A. DiAntonio, and J. Milbrandt. 2016. SARM1-specific motifs in the TIR domain enable NAD<sup>+</sup> loss and regulate injury-induced SARM1 activation. *Proc. Natl. Acad. Sci. USA.* 113:E6271–E6280. <https://doi.org/10.1073/pnas.1601506113>
- Sumner, C.J., and T.O. Crawford. 2018. Two breakthrough gene-targeted treatments for spinal muscular atrophy: challenges remain. *J. Clin. Invest.* 128:3219–3227. <https://doi.org/10.1172/JCI121658>
- Szretter, K.J., M.A. Samuel, S. Gilfillan, A. Fuchs, M. Colonna, and M.S. Diamond. 2009. The immune adaptor molecule SARM modulates tumor necrosis factor alpha production and microglia activation in the brainstem and restricts West Nile Virus pathogenesis. *J. Virol.* 83:9329–9338. <https://doi.org/10.1128/JVI.00836-09>
- Tagliaferro, P., and R.E. Burke. 2016. Retrograde Axonal Degeneration in Parkinson Disease. *J. Parkinsons Dis.* 6:1–15. <https://doi.org/10.3233/JPD-150769>
- Turkiew, E., D. Falconer, N. Reed, and A. Höke. 2017. Deletion of Sarm1 gene is neuroprotective in two models of peripheral neuropathy. *J. Peripher. Nerv. Syst.* 22:162–171. <https://doi.org/10.1111/jns.12219>
- Wang, M.S., G. Fang, D.G. Culver, A.A. Davis, M.M. Rich, and J.D. Glass. 2001. The WldS protein protects against axonal degeneration: a model of gene therapy for peripheral neuropathy. *Ann. Neurol.* 50:773–779. <https://doi.org/10.1002/ana.10039>
- Wang, M.S., A.A. Davis, D.G. Culver, and J.D. Glass. 2002. WldS mice are resistant to paclitaxel (taxol) neuropathy. *Ann. Neurol.* 52:442–447. <https://doi.org/10.1002/ana.10300>
- Yang, J., Z. Wu, N. Renier, D.J. Simon, K. Uryu, D.S. Park, P.A. Greer, C. Tournier, R.J. Davis, and M. Tessier-Lavigne. 2015. Pathological axonal death through a MAPK cascade that triggers a local energy deficit. *Cell.* 160:161–176. <https://doi.org/10.1016/j.cell.2014.11.053>
- Yin, T.C., J.R. Voorhees, R.M. Genova, K.C. Davis, A.M. Madison, J.K. Britt, C.J. Cintrón-Pérez, L. McDaniel, M.M. Harper, and A.A. Pieper. 2016. Acute Axonal Degeneration Drives Development of Cognitive, Motor, and Visual Deficits after Blast-Mediated Traumatic Brain Injury in Mice. *eNeuro.* 3:ENEURO.0220-16.2016. <https://doi.org/10.1523/ENEURO.0220-16.2016>
- Ziogas, N.K., and V.E. Koliatsos. 2018. Primary Traumatic Axonopathy in Mice Subjected to Impact Acceleration: A Reappraisal of Pathology and Mechanisms with High-Resolution Anatomical Methods. *J. Neurosci.* 38:4031–4047. <https://doi.org/10.1523/JNEUROSCI.2343-17.2018>